Reduced aliasing artifacts using shaking projection *k*-space sampling trajectory*

Zhu Yan-Chun(朱艳春)[a], Du Jiang(杜 江)[b], Yang Wen-Chao(杨文超)[a)c)], Duan Chai-Jie(段侪杰)[d], Wang Hao-Yu(王浩宇)[a], Gao Song(高 嵩)[a)e)†], and Bao Shang-Lian(包尚联)[a)‡]

[a)] *Beijing Key Laboratory of Medical Physics and Engineering, School of Physics, Peking University, Beijing* 100871, *China*
[b)] *Department of Radiology, University of California, San Diego, CA* 92103-8226, *USA*
[c)] *Institute of Computational Physics and Complex Systems, Lanzhou University, Lanzhou* 730000, *China*
[d)] *Shenzhen Key Laboratory for Minimal Invasive Medical Technologies, Tsinghua University, Shenzhen* 518055, *China*
[e)] *Medical Imaging Physics Laboratory, Health Science Center of Peking University, Beijing* 100191, *China*

(Received 16 December 2013; revised manuscript received 7 January 2014; published online 24 January 2014)

Radial imaging techniques, such as projection-reconstruction (PR), are used in magnetic resonance imaging (MRI) for dynamic imaging, angiography, and short-T2 imaging. They are less sensitive to flow and motion artifacts, and support fast imaging with short echo times. However, aliasing and streaking artifacts are two main sources which degrade radial imaging quality. For a given fixed number of *k*-space projections, data distributions along radial and angular directions will influence the level of aliasing and streaking artifacts. Conventional radial *k*-space sampling trajectory introduces an aliasing artifact at the first principal ring of point spread function (PSF). In this paper, a shaking projection (SP) *k*-space sampling trajectory was proposed to reduce aliasing artifacts in MR images. SP sampling trajectory shifts the projection alternately along the *k*-space center, which separates *k*-space data in the azimuthal direction. Simulations based on conventional and SP sampling trajectories were compared with the same number projections. A significant reduction of aliasing artifacts was observed using the SP sampling trajectory. These two trajectories were also compared with different sampling frequencies. A SP trajectory has the same aliasing character when using half sampling frequency (or half data) for reconstruction. SNR comparisons with different white noise levels show that these two trajectories have the same SNR character. In conclusion, the SP trajectory can reduce the aliasing artifact without decreasing SNR and also provide a way for undersampling reconstruction. Furthermore, this method can be applied to three-dimensional (3D) hybrid or spherical radial *k*-space sampling for a more efficient reduction of aliasing artifacts.

Keywords: shaking projection, radial sampling, gridding reconstruction, point spread function

PACS: 87.61.–c, 87.15.A–, 87.57.C– **DOI:** 10.1088/1674-1056/23/3/038702

1. Introduction

Nowadays, more and more new techniques have been put forward in the magnetic resonance imaging (MRI) area, which contain hardware improvement[1,2] and theoretical innovation.[3] Projection acquisition (also called radial acquisition) has been used since the beginning in MRI.[4] With recent advances in gradient hardware and sequence design, rapid imaging has become one of the most important objectives in clinical applications. There are essentially two ways to increase imaging speed: a faster scanning of *k*-space or a reduction in *k*-space coverage.[5] Rapid *k*-space traverse is hardware dependent, and reduced *k*-space coverage always introduces artifact and reduces the signal to noise ratio (SNR).

Radial sampling has advantages of shorter echo times, less sensitivity to motion, and higher temporal resolution for some applications.[6] Some applications, such as time-resolved contrast enhanced magnetic resonance angiography (CE-MRA),[7,8] are quite tolerable to angular undersampling. A high temporal resolution can be achieved without spatial resolution reduction and much streak artifact. However, most radial sampling techniques are subject to aliasing and streaking artifacts[9] which may significantly degrade the image quality. In recent years, a variety of advanced radial sampling techniques have been proposed to address these challenges.

MR imaging suffers aliasing artifacts[10] when the excited object exceeds the prescribed field of view (FOV). There are some methods to overcome the aliasing problem by selective excitation or selective saturation. The multidimensional selective excitation pulse[11] was designed to excite only spins in the region of interest (ROI). However, the actual implementation of such a pulse may be difficult for some specific ROI shapes. Selective saturation pulses to presaturate spins outside the ROI[12] are used before the primary sequence to decrease the aliasing artifact. However, the minimum repetition time (TR) is prolonged and the steady state of spins within the ROI may be corrupted if the saturation pulses are not used in ev-

*Project supported by the National Basic Research Program of China (Grant No. 2011CB707701), the Innovation Fund for Technology Based Firms, China (Grant No. 11C26221103870), the National High Technology Research and Development Program of China (Grant Nos. 2011BAI12B05 and 2011BAI23B07), the National Natural Science Foundation of China (Grant Nos. 81171330, 81271664, and 81230035).

†Corresponding author. E-mail: gaoss@bjmu.edu.cn
‡Corresponding author. E-mail: bao@pku.edu.cn

© 2014 Chinese Physical Society and IOP Publishing Ltd

ery TRs. Some studies overcome the aliasing problem with modified k-space trajectories. Nayak *et al*[13] showed that randomized trajectories could disrupt the coherence of aliasing artifacts. However, truly randomized trajectories[14] are difficult to implement on a scanner. Variable sample densities[15,16] from k-space center to edge in spiral and cartesian trajectories were used to decrease the aliasing artifact. However, such trajectories are not used in radial trajectory.

In this paper, we put forward a novel radial k-space sampling pattern, which shakes projections alternately (as shown in Fig. 1). The simulation samplings k-space data of SP and conventional trajectories were reconstructed by using gridding algorithms. PSFs were also generated to describe the trajectory difference. Aliasing artifacts were compared between these two sampling patterns. Compared with the conventional radial k-space trajectory, the SP trajectory was proved to decrease the aliasing artifact when using the same number of data. These two trajectories were also compared with different sampling frequencies. SP trajectory has the same aliasing character when using a half sampling frequency (or half data) for reconstruction. SNR simulation with different white noise levels showed that these two trajectories have similar SNR results. In conclusion, the SP trajectory is a good way to reduce the aliasing artifact without SNR decrease and can apply for undersampling reconstruction.

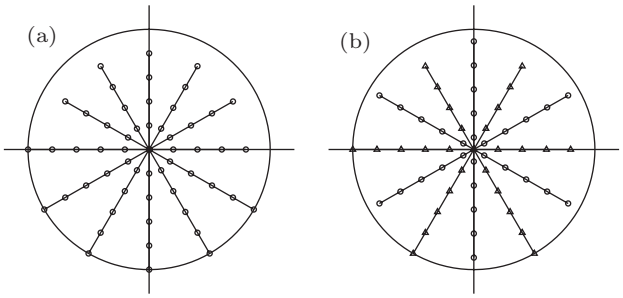


Fig. 1. Illustration of conventional sampling trajectory (a) and SP sampling trajectory (b). The graphic uses six projections and ten samples in the radial direction for illustration only. The projections with triangle points pass through k-space center, and projections with circle points shift $\Delta k_r/2$ relatively. These two patterns of projections alternate in the azimuthal direction.

2. Model and method

2.1. SP sampling pattern

In this method, k-space is scanned on a radial polar grid. SP sampling trajectory shifts the projection alternately along the k-space center, as shown in Fig. 1(b). The projections with triangle points pass through the k-space center, and projections with circle points shift $\Delta k_r/2$ relatively. These two patterns of projections alternate in the azimuthal direction. Compared with the conventional sampling trajectory (as shown in Fig. 1(a)), data points in the azimuthal direction separate into double circles in the SP trajectory. The SP trajectory can be considered as two trajectories, a triangle point trajectory and a circle point trajectory. The circle point projection is symmetrically divided by k-space center and without k-space center sampled.

2.2. Theory

MR images are reconstructed from a limited number of k-space samples. The resulting image degradation is usually described by PSF of the corresponding sampling trajectory.[17–19] The image reconstructed from a sampling trajectory is the original image convolved with the corresponding PSF. The conventional radial sampling function $S(k_r,k_\theta)$ (Fig. 1(a)) is a sum over the product of two delta functions as

$$\begin{aligned} &S(k_r,k_\theta)\\ &= \Delta k_\theta \Delta k_r \sum_{n_\theta=0}^{N_\theta-1} \sum_{n_r=-N_r/2}^{N_r/2-1} \delta(k_\theta - n_\theta \Delta k_\theta)\delta(k_r - n_r \Delta k_r), \end{aligned} \quad (1)$$

where N_θ is the number of projections separated by the angular increment of $\Delta k_\theta = \pi/N_\theta$, and N_r is the number of samples in the k_r direction with radial increment Δk_r. The sampling function of the SP sampling trajectory (Fig. 1(b)) can be written as

$$\begin{aligned} &S(k_r,k_\theta)\\ &= S_\triangle(k_r,k_\theta) + S_\odot(k_r,k_\theta)\\ &= \Delta k_\theta \Delta k_r \sum_{n_\theta=0}^{N_\theta/2-1} \sum_{n_r=-N_r/2}^{N_r/2-1} [\delta(k_\theta - 2n_\theta \Delta k_\theta)\delta(k_r - n_r \Delta k_r)\\ &\quad + \delta(k_\theta - (2n_\theta+1)\Delta k_\theta)\delta(k_r - (n_r+1/2)\Delta k_r)]. \end{aligned} \quad (2)$$

The resulting PSF is given as

$$\begin{aligned} &\mathrm{PSF}(r,\theta)\\ &= \int_{k_\theta=0}^{\pi} \int_{k_r=-\infty}^{k_r=+\infty} S(k_r,k_\theta)\, \mathrm{e}^{2\pi \mathrm{i} r k_r \cos(k_\theta-\theta)} |k_r| \,\mathrm{d}k_\theta \,\mathrm{d}k_r \end{aligned} \quad (3)$$

by the Fourier transformation in polar coordinates of the sampling function $S(k_r,k_\theta)$. The SP sampling pattern has the same angular increment Δk_θ and projections N_θ with conventional sampling pattern and is expected to have nearly the same streaking artifact level. Continuous sampling in an angular direction was investigated by Lauzon and Rutt.[19] For this ring-like sampling, equation (3) reduces to

$$\mathrm{PSF}(r) = \frac{\pi(\Delta k_r)^2}{4} + 2\pi(\Delta k_r)^2 \sum_{n_r=1}^{N_r/2-1} n_r \mathrm{J}_0(2\pi \Delta k_r n_r r), \quad (4)$$

which is a sum over the zeroth-order Bessel functions J_0. Discretization by Δk_r in the radial direction leads to radial ring lobes at $r = j/\Delta k_r$, $j = 1,2,\ldots$. The concentric ring lobes surrounding the main peak at $r = 0$ are responsible for the radial aliasing artifact.

Assume that we sample nearly continuously in the angular direction, therefore, the PSF of sampling function Eq. (2) reduces to

$$\begin{aligned}&\mathrm{PSF}(r)\\ &= \frac{1}{2}[\mathrm{PSF}_{\triangle}(r)+\mathrm{PSF}_{\odot}(r)]\\ &= \frac{1}{2}\left[\frac{\pi(\Delta k_r)^2}{4}+2\pi(\Delta k_r)^2\sum_{n_r=1}^{N_r/2-1} n_r \mathrm{J}_0(2\pi\Delta k_r n_r r)\right.\\ &\left.+2\pi(\Delta k_r)^2\sum_{n_r=1}^{N_r/2}\left(n_r-\frac{1}{2}\right)\mathrm{J}_0\left(2\pi\Delta k_r\left(n_r-\frac{1}{2}r\right)\right)\right]. \quad (5)\end{aligned}$$

For conventional radial sampling, the aliasing artifact occurs when the object size exceeds the circular FOV with a diameter of $1/\Delta k_r$. From Eq. (4), $\mathrm{PSF}(1/\Delta k_r)$ of conventional trajectory is calculated as

$$\mathrm{PSF}\left(\frac{1}{\Delta k_r}\right)_{\mathrm{C}} = \frac{\pi(\Delta k_r)^2}{4}+2\pi(\Delta k_r)^2\sum_{n_r=1}^{N_r/2-1} n_r \mathrm{J}_0(2\pi n_r), \quad (6)$$

where C denotes the conventional trajectory. High intensity will generate at $r = 1/\Delta k_r$ based on zero-order Bessel function J_0 character. This bright ring always brings a heavy aliasing artifact especially in undersampling radial k-space. Likewise, $\mathrm{PSF}(1/\Delta k_r)$ of the SP sampling trajectory is shown as

$$\begin{aligned}&\mathrm{PSF}\left(\frac{1}{\Delta k_r}\right)_{\mathrm{SP}}\\ &= \frac{\pi(\Delta k_r)^2}{8}+\pi(\Delta k_r)^2\sum_{n_r=1}^{N_r/2-1} n_r \mathrm{J}_0(2\pi n_r)\\ &+\pi(\Delta k_r)^2\sum_{n_r=1}^{N_r/2-1}(n_r-1/2)\mathrm{J}_0(2\pi(n_r-1/2)). \quad (7)\end{aligned}$$

Based on the oscillation character of Bessel function J_0, part two and part three in Eq. (7) are opposite in sign. Therefore, a smaller PSF value can be generated around $r = 1/\Delta k_r$. This is expected to cause a lower aliasing artifact.

2.3. Gridding reconstruction

MRI acquisitions using radial trajectories are usually reconstructed with either back projection reconstruction or regridding methods.[20] Gridding is more popular for reconstructing data from nonrectilinear k-space trajectories.[21,22] The gridding algorithm can be divided into two stages: sampling density compensation and inverse Fourier transform. In the gridding algorithm, the inverse Fourier transform is estimated by convolving the density compensated data with a finite kernel, sampling onto a Cartesian grid, performing an FFT and multiplying by an apodization correction function. Jackson *et al* examined many different functions that could be used for gridding kernels and found the Kaiser–Bessel window preferable since it is easy to compute and offers near optimal performance.[21]

The collected data must be properly weighted before interpolation.[23] We used the area of the Voronoi cell around each sample as a measure for its spatial extent.[24] As shown in Fig. 2, the density weighting of each sampling point outside $k = 0$ was calculated by its sector area. The areas of points at $k = 0$ was calculated by two symmetrical sectors with radius of $\Delta k_r/2$. A Kaiser–Bessel kernel with a window size $w = 4$ and $\beta = 18.5547$ was used with typically grid oversampling ratio $\alpha = 2$.[21]

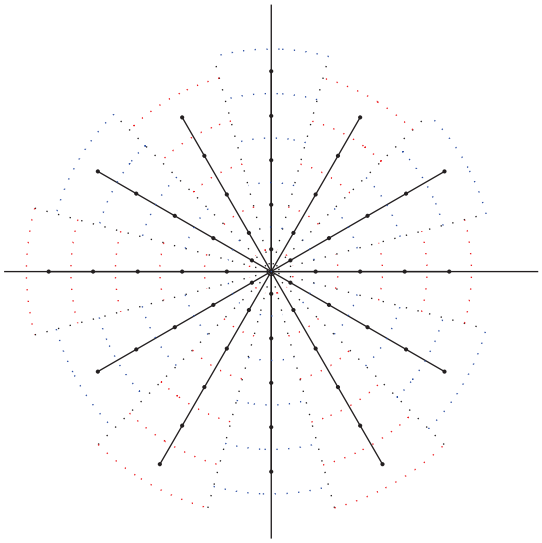


Fig. 2. Density weight of each sampling point by using the Voronoi cell area of each sample. Each sampling point outside $k = 0$ was calculated by its sector area. The areas of points at $k = 0$ were calculated by two symmetrical sectors with radius of $\Delta k_r/2$.

2.4. Sampling simulation

Based on the well-known Nyquist criterion, $\pi n/2$ projections have to be obtained for an image with a base resolution of $n \times n$ sample points. In order to compare the aliasing artifact, both the conventional and SP patterns were set to satisfy the Nyquist condition. 402 projections (256 samples each) were sampled from the Shepp–Logan phantom. The simulations were written using Matlab (MathWorks, Natick, MA). Reconstructed images with matrix 256×256 were cut from the gridding reconstructed images with a matrix of 512×512. Differences with the original Shepp–Logan phantom image were calculated after normalization. The aliasing artifact power (AP)[27] was calculated in these two methods using the following equation:

$$\mathrm{AP} = \frac{\sum_j \| I_j^{\mathrm{ref}} | - | I_j^{\mathrm{recon}} \|^2}{\sum_j | I_j^{\mathrm{ref}} |^2}, \quad (8)$$

where j is a pixel index, I^{ref} is the original phantom image, and I^{recon} are the reconstructed images from these two methods. Note that a higher value of AP represents increased artifacts and reduced image quality.

In PSF image of radial sampling, bright rings in the PSF induce aliasing artifacts. The locations of these rings satisfy $\Delta k_r \mathrm{FOV} = n$, where n is the number of bight rings. In order to present more ring lobes, we choose a sampling matrix of 201 projections (128 samples each) and generate a PSF image matrix of 512×512 in PSF comparison.

2.5. Noise simulation

Compared with the conventional radial sampling trajectory, half number of projections in SP trajectory were sampled without k-space centers. This may influence the SNR of the image. To investigate the SNR character of the SP trajectory, the noise simulation has been done by adding the same level of white noise to these two trajectories k-space data.[25] Different noise levels from -20 dB to -40 dB were used in the simulation. Since undersampling will induce the streaking artifacts, fully sampling (402 projections) was used in the noise simulation. The SNRs from different noise levels were calculated. In order to eliminate aliasing artifact degradation, images with different noise levels were subtracted by the noise free image from each trajectory, and the differences were used to calculate the image noise. The bright ellipse edge was used to calculate as a signal. The SNR was calculated using the following equation:

$$\mathrm{SNR} = \sqrt{2}\frac{\bar{I}}{\sigma}. \tag{9}$$

2.6. Different sampling bandwidth simulation

From the PSF formula (4), we know that the value of $\Delta k_r r$ effects the aliasing artifact location. If we double the value of Δk_r, an aliasing artifact will appear at location $r = \mathrm{FOV}/2$. Doubling the sampling step size means using a half sampling bandwidth. Decreasing the sampling bandwidth can decrease electronic noise. In this simulation, these two trajectories were sampled with steps $\Delta k_r = 1$ and $\Delta k_r = 2$ individually. The same FOV was used in these simulations.

3. Results

3.1. Sampling simulation results

Shepp–Logan phantom was used in the simulation. Full sampling with 402 projections (256 samples each) was used in both trajectories to eliminate the streaking artifact. After regridding the reconstruction, the images from these two sampling trajectories were obtained as shown in Figs. 3(a) and 3(c). Although we used oversampling in the reconstruction that the aliasing artifact was not overlapped on the phantom, the aliasing artifacts still appeared at the corners of the conventional trajectory generated image (as shown in Fig. 3(a)). However, in the image generated by SP trajectories, aliasing artifacts disappeared. In order to compare these two reconstructed images, the images were normalized before being displayed in the same gray level. Clearly differences were seen by subtracting these two reconstructed images from the original phantom image after normalization (as shown in Figs. 3(b) and 3(d)). Obvious aliasing artifact elimination can be found by comparing Figs. 3(c) and 3(d). The aliasing AP of a conventional trajectory is 0.1208 and the SP trajectory is 0.0176. Significant improvement (nearly 7 times) in the aliasing artifact is found in images acquired with the SP trajectory.

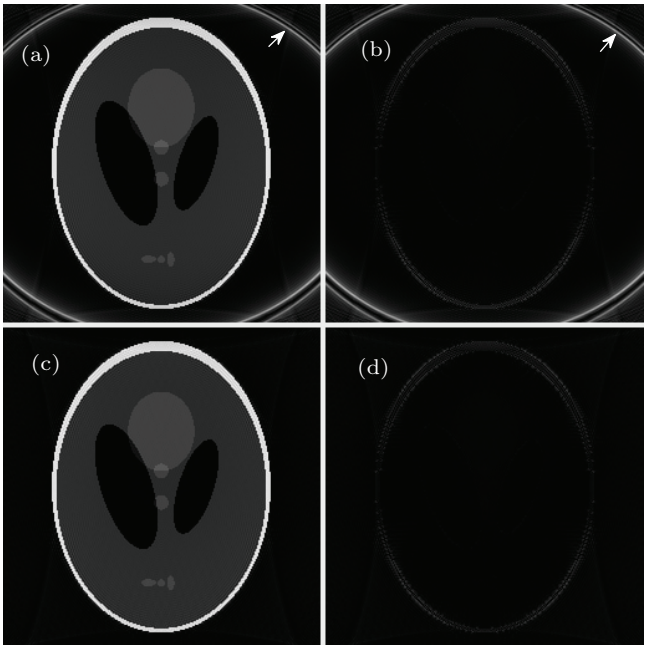


Fig. 3. Shepp–Logan phantom images were reconstructed from conventional (a) and SP (c) trajectories. (b) and (d) show the difference between the original fully sampled Shepp–Logan phantom image and the newly reconstructed images acquired with conventional and SP trajectories, respectively.

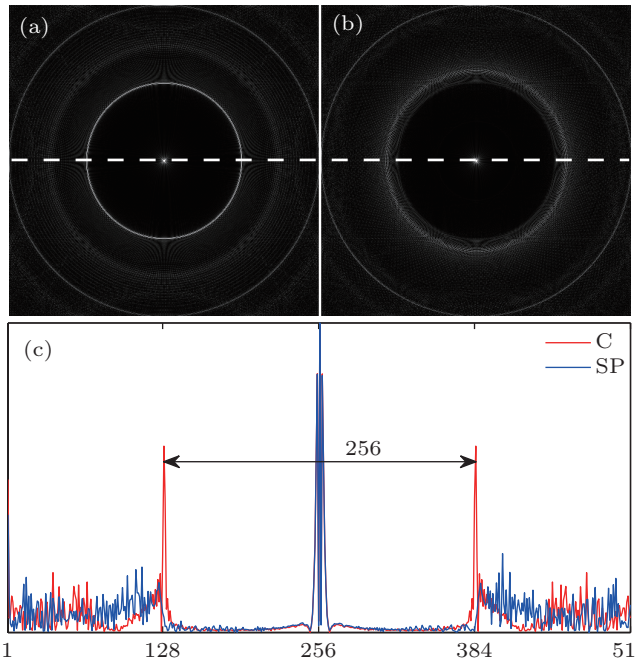


Fig. 4. (color online) PSF comparison between these two sampling trajectories. PSF image was generated from full sampling k-space with 201 projections and 128 points on each projection. (a) shows PSF reconstructed from the conventional sampling trajectory, and (b) shows the reconstructed PSF from the SP sampling trajectory. The centerlines of these two PSFs are shown in panel (c). The red line is conventional and blue line is the SP trajectory.

In PSF comparison, in order to show more aliasing ring lobes in the PSF image, PSF was generated using a smaller sampling matrix with 201 projections (128 samples each) and a reconstructed image matrix of 512×512. Figures 4(a) and 4(b) show PSFs reconstructed from conventional and SP sampling trajectories. In comparison, we found that the first principle ring of PSF from the SP trajectory was diluted and spread out. The center line of PSFs were extracted as shown in Fig. 4(c). The bright circle of the conventional method PSF has a higher amplitude than the SP method. The effective FOV of the SP trajectory was bigger than that of the conventional trajectory. The amplitude of PSF around the first bright ring oscillate sharply in the SP trajectory, which was caused by the summation of part two and part three in Eq. (7). With such PSF in convolution, the reconstruction got an aliasing artifact free image.

3.2. Noise simulation results

Different white noise levels from −20 dB to −40 dB were added to *k*-space data as the electronic noise. The mean amplitude value of bright ellipse edge of Shepp–Logan phantom was calculated as a signal, and the difference between noise image and noise free image was calculated as a noise value. The signal and noise change as added noise levels are shown in Figs. 5(a) and 5(b). The SNR changing with different noise levels is shown in Fig. 5(c). Signals of the SP trajectory were a little higher than the conventional trajectory (1.3%). Noises of these two trajectories were increasing as more white noise was added. However, noises from the conventional trajectory increase faster than that from the SP trajectory. SNRs calculated from Eq. (8) were similar. The SNR of the SP trajectory is 7.8% higher than that of the conventional trajectory.

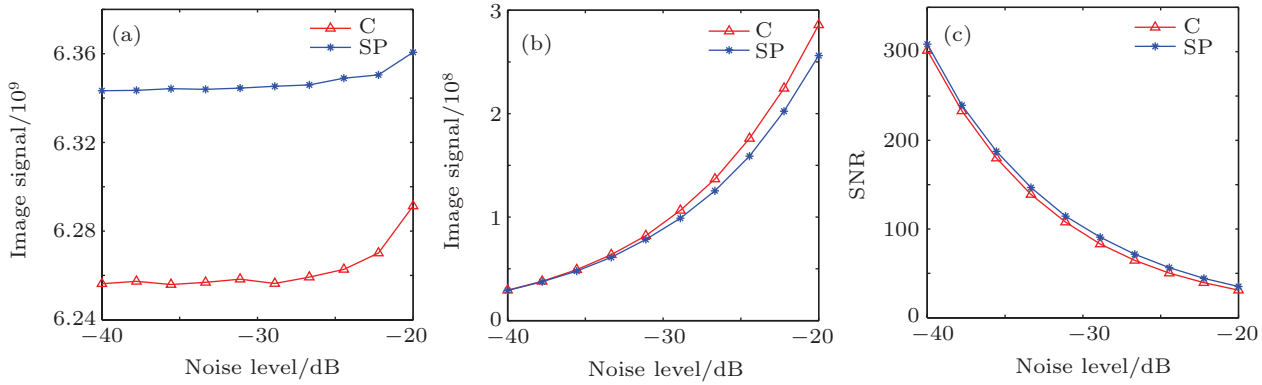


Fig. 5. (color online) Noise simulations with different noise levels (−40 dB–−20 dB) added to full sampling trajectories. Signals were calculated from bright ellipse edge of phantom (a), and noises were calculated from subtraction images (b). The SNR of the SP method is 7.8% higher than that of the conventional trajectory (c).

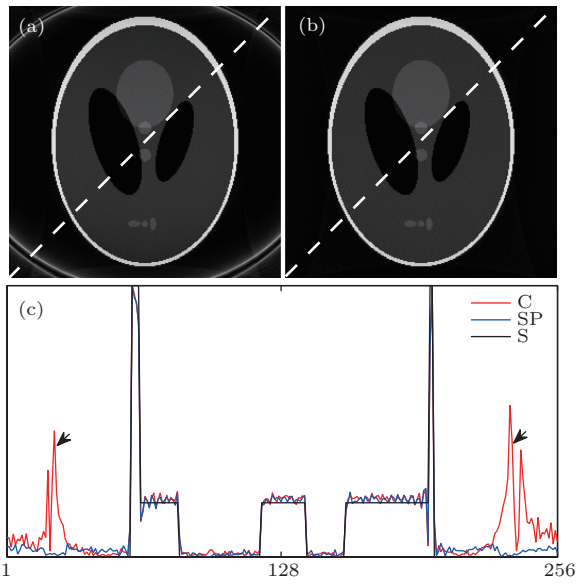


Fig. 6. (color online) Images with −40-dB noise added to the *k*-space of conventional and SP trajectories ((a) and (b)). (c) shows the signals compared with the standard phantom along the across dotted lines. The black lines in panel (c) are from the standard phantom signal, and red and blue lines are from conventional and SP trajectories generated images, respectively.

Figures 6(a) and 6(b) show image comparisons when −40-dB noise was added to *k*-space of conventional and SP trajectories. Signals along the oblique dotted lines are shown in Fig. 6(c). Standard phantom signal along that line is present as a black line in Fig. 6(c). Aliasing artifact amplitudes are shown in Fig. 6(c) as arrow points. Except the aliasing artifacts difference, similar noise performances are seen in these two methods.

3.3. Different sampling bandwidth simulation results

Figure 7 was the results with different sampling bandwidths. The left column images (as shown in Figs. 7(a) and 7(c)) were simulated with sampling steps $\Delta k_r = 1$ and 2 for the right column images. The upper row images (Figs. 7(a) and 7(b)) are the conventional trajectory and the lower row is the SP trajectory. The aliasing artifact in the conventional trajectory image (Fig. 6(a)) was very bright and gathering to the center when the sampling step was doubled. The same phenomenon was seen in the SP trajectory, but the aliasing artifact did not contaminate the phantom image. The image of the SP trajectory with sampling step of 2 was similar to that

when using a conventional trajectory with a sampling step of 1. This means that we can obtain a similar image using the half sampling bandwidth in the SP trajectory. Using a half sampling bandwidth can also improve the SNR by decreasing the electronic noise.

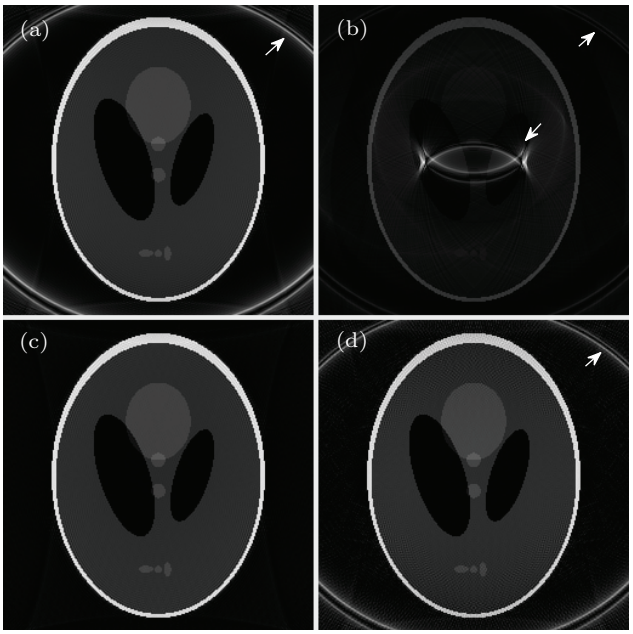


Fig. 7. Comparison of different sampling bandwidths. (a) and (b) reconstructed from the conventional trajectory and (c) and (d) reconstructed from the SP trajectory. The right side images were sampled with a half bandwidth that compared with the left side images. The image from the SP trajectory with a half bandwidth has a similar aliasing character as that of the conventional trajectory.

4. Discussion

The phantom studies show that the SP trajectory is able to decrease the aliasing artifact effectively. Usually, the aliasing artifact can be decreased by increasing the FOV or increasing the sampling points (the same as decreasing the sampling step). The novel method increases neither the scan time nor the reconstruction time, but can reduce the aliasing artifact in the final image. Therefore, with the same aliasing artifact standard requirement, the novel radial sampling pattern provides an option to use a low sampling bandwidth or short echo time. In addition, this method can decrease the noise by using the low sampling bandwidth.

In the SP trajectory, half k-space center ($k = 0$) data points were not sampled. However, the SNR of the SP trajectory was a little higher than that of the conventional trajectory. The reason for signal gain in the SP trajectory may be that the k-space center ($k = 0$) has already been oversampled in both trajectories. More data sampled around $k = 0$ instead of only oversampling the $k = 0$ point will be better for image quality. In reality, a nonlinear projection with non-equidistance data points was usually used. In these projections, more k-space data around the center were sampled and less in the edge.[16] Such projections can also be combined with the shaking projections technique as necessary.

In a given fixed number of data points radial k-space sampling, the data in the angular and radial direction distributions affect the streaking and aliasing artifact levels.[5] Too many data distributed along the angular direction and fewer circles in the radial direction will cause an aliasing artifact. On the contrary, too many data lying along the radial direction and fewer projections will cause a streaking artifact. The novel k-space sampling method increases cycles in the radial direction with the same projection number. It makes the data distributed more discrete in the radial direction. Based on the same idea, more and more novel k-space sampling methods will be designed not only in radial but also in spiral or other trajectories.

The novel sampling method can also be extended to three-dimensional (3D) imaging that uses either a cylindrical k-space volume with a stack of 2D radial projections combined with Cartesian encoding in the slice direction (hybrid radial)[28] or a spherical k-space volume with 3D radial projections.[29] In addition, shaking projections can also be used in TWIRL[30] and WHIRL,[31] which combine radial and spiral trajectories. Additional simulation and research are needed in other k-space sampling trajectories and applications.

5. Conclusion

In conclusion, the SP trajectory can decrease the aliasing artifact effectively and without SNR decrease and also provide a way for undersampling reconstruction. Furthermore, this novel sampling method can also be extend to 3D imaging trajectories and other 2D trajectories. Additional simulation and research are needed in other k-space samplings and applications.

References

[1] Tang X, Hong L M and Zu D L 2010 *Chin. Phys. B* **19** 078702
[2] Xu Y, Wang W T and Wang W M 2012 *Chin. Phys. B* **21** 118704
[3] Zu Z L, Zhou K, Zhang S G, Gao S and Bao S L 2008 *Chin. Phys. B* **17** 328
[4] Lauterbur P C 1973 *Nature* **242** 190
[5] Scheffler K and Hennig J 1998 *Magn. Reson. Med.* **40** 474
[6] Bao S L, Du J and Gao S 2013 *Acta. Phys. Sin.* **62** 088701 (in Chinese)
[7] Du J, Carroll T, Block W, Fain S, Korosec F, Grist T and Mistretta C 2003 *Magn. Reson. Med.* **49** 909
[8] Du J, Carroll T, Wagner H, Vigen K, Fain S, Block W, Korosec F, Grist T and Mistretta C 2002 *Magn. Reson. Med.* **48** 516
[9] Joseph P M 1998 *Magn. Reson. Med.* **40** 460
[10] Pusey E, Yoon C, Anselmo M L and Lufkin R B 1988 *Comput. Med. Imaging Graph.* **12** 219
[11] Pauly J, Nishimura D and Macovski A 1989 *J. Magn. Reson.* **81** 43
[12] Singh S, Rutt B K and Mark Henkelman R 1990 *J. Magn. Reson.* **87** 567
[13] Nayak K S and Nishimura D G 1998 *Proceedings of the* 6*th Annual Meeting of the International Society for Magnetic Resonance in Medicine*, April 1–7, 1998, Sydney, p. 670
[14] Scheffler K and Hennig J 1996 *Magn. Reson. Med.* **35** 569
[15] Fang S, Wu W C, Ying K and Guo H 2013 *Acta. Phys. Sin.* **62** 048702
[16] Tsai C M and Nishimura D G 2000 *Magn. Reson. Med.* **43** 452
[17] Pipe J G 2000 *Magn. Reson. Med.* **43** 867

[18] Larson P, Gurney P and Nishimura D 2008 *IEEE Trans. Med. Imaging* **27** 47

[19] Lauzon M and Rutt B 1996 *Magn. Reson. Med.* **36** 940

[20] Lauzon M and Rutt B 1998 *Magn. Reson. Med.* **40** 769

[21] Jackson J I, Meyer C H, Nishimura D G and Macovski A 1991 *IEEE Trans. Med. Imaging* **10** 473

[22] Beatty P J, Nishimura D G and Pauly J M 2005 *IEEE Trans. Med. Imaging* **24** 799

[23] Pipe J G and Menon P 1999 *Magn. Reson. Med.* **41** 179

[24] Rasche V, Proksa R, Sinkus R, Bornert P and Eggers H 1999 *IEEE Trans. Med. Imaging* **18** 385

[25] Wang H Y, Hu J N, Xie Y Q, Chen J, Yu A, Wei X H, Dai Y M, Li M, Bao S L and Haacke E M 2013 *Chin. Phys. B* **22** 038702

[26] McRobbie D W, Moore E A, Graves M J and Prince M R 2007 *MRI from Picture to Proton* (New York: Cambridge University Press) p. 202

[27] McKenzie C A, Yeh E N and Sodickson D K 2001 *Magn. Reson. Med.* **46** 831

[28] Peters D, Korosec F, Grist T, Block W, Holden J, Vigen K and Mistretta C 2000 *Magn. Reson. Med.* **43** 91

[29] Glover G and Pauly J 1992 *Magn. Reson. Med.* **28** 275

[30] Jackson J I, Nishimura D and Macovski A 1992 *Magn. Reson. Med* . **25** 128

[31] Pipe J G 1999 *Magn. Reson. Med.* **42** 714